



Dimethyl Fumarate Blocks Tumor Necrosis Factor-Alpha-Driven Inflammation and Metabolic Rewiring in the Retinal Pigment Epithelium

Daisy Y. Shu^{1,2}, Scott I. Frank¹, Tessa C. Fitch¹, Margarete M. Karg^{1,2}, Erik R. Butcher¹, Emmanuella Nnuji-John^{1,3}, Leo A. Kim^{1,2} and Magali Saint-Geniez^{1,2*}

¹ Schepens Eye Research Institute of Massachusetts Eye and Ear, Boston, MA, United States, ² Department of Ophthalmology, Harvard Medical School, Boston, MA, United States, ³ Cold Spring Harbor Laboratory, School of Biological Sciences, Cold Spring Harbor, NY, United States

OPEN ACCESS

Edited by:

Henri Leinonen,
University of Eastern Finland, Finland

Reviewed by:

Kai Kaarniranta,
University of Eastern Finland, Finland
Dorota Skowronska-Krawczyk,
UCI Health, United States

*Correspondence:

Magali Saint-Geniez
msaintgeniez@gmail.com

Specialty section:

This article was submitted to
Brain Disease Mechanisms,
a section of the journal
Frontiers in Molecular Neuroscience

Received: 15 March 2022

Accepted: 25 May 2022

Published: 23 June 2022

Citation:

Shu DY, Frank SI, Fitch TC,
Karg MM, Butcher ER, Nnuji-John E,
Kim LA and Saint-Geniez M (2022)
Dimethyl Fumarate Blocks Tumor
Necrosis Factor-Alpha-Driven
Inflammation and Metabolic Rewiring
in the Retinal Pigment Epithelium.
Front. Mol. Neurosci. 15:896786.
doi: 10.3389/fnmol.2022.896786

The retinal pigment epithelium (RPE) acts as a metabolic gatekeeper between photoreceptors and the choroidal vasculature to maintain retinal function. RPE dysfunction is a key feature of age-related macular degeneration (AMD), the leading cause of blindness in developed countries. Inflammation is a key pathogenic mechanism in AMD and tumor necrosis factor-alpha (TNF α) has been implicated as a pro-inflammatory cytokine involved in AMD. While mitochondrial dysfunction has been implicated in AMD pathogenesis, the interplay between inflammation and cellular metabolism remains elusive. The present study explores how the pro-inflammatory cytokine, TNF α , impacts mitochondrial morphology and metabolic function in RPE. Matured human primary RPE (H-RPE) were treated with TNF α (10 ng/ml) for up to 5 days. TNF α -induced upregulation of IL-6 secretion and inflammatory genes (IL-6, IL-8, MCP-1) was accompanied by increased oxidative phosphorylation (OXPHOS) and reduced glycolysis, leading to an increase in cellular adenosine triphosphate (ATP) content. Transmission electron microscopy (TEM) revealed defects in mitochondrial morphology with engorged mitochondria and loss of cristae integrity following TNF α treatment. Pre-treatment with the anti-inflammatory drug, 80 μ M dimethyl fumarate (DMFu), blocked TNF α -induced inflammatory activation of RPE (IL-6, IL-8, MCP-1, CFH, CFB, C3) and normalized their bioenergetic profile to control levels by regulating PFKFB3 and PKM2 gene expression. Furthermore, DMFu prevented TNF α -induced mitochondrial dysfunction and morphological anomalies. Thus, our results indicate that DMFu serves as a novel therapeutic avenue for combating inflammatory activation and metabolic dysfunction of RPE in AMD.

Keywords: inflammation, metabolism, mitochondria, retinal pigment epithelium, tumor necrosis factor-alpha, oxidative phosphorylation, glycolysis, age-related macular degeneration

INTRODUCTION

Dysfunction of retinal pigment epithelial cells (RPE) is an early sign of AMD and loss of RPE integrity increases as AMD progresses (Bonilha, 2008; Ao et al., 2018). Inflammation is a key pathogenic mechanism in AMD (Datta et al., 2017) through complement system activation, upregulation of inflammatory cytokines and recruitment of macrophages to the outer surface of the RPE-Bruch's membrane interface in AMD eyes (Hageman et al., 2001) that facilitates drusen growth (Levy et al., 2015). A critical cytokine mediating inflammatory responses throughout the body is tumor necrosis factor- α (TNF α), which has been implicated in the pathogenesis of AMD (Oh et al., 1999; Wan et al., 2010; Kutty et al., 2016). Single nucleotide polymorphisms (SNPs) have been detected in the TNF α gene in AMD patients (Wan et al., 2010; Chernykh et al., 2019) and TNF α decreases the expression of genes regulating RPE function, including RPE65 (Kutty et al., 2016). Further, lower serum levels of TNF α have been associated with improved visual acuity after anti-VEGF therapy in wet AMD patients (Khan et al., 2021), highlighting TNF α as a pathogenic driver of wet AMD.

Defects in RPE mitochondria and metabolism drive AMD pathogenesis (Fisher and Ferrington, 2018; Kaarniranta et al., 2020; Zhang et al., 2020). Work in our laboratory has further implicated metabolic and mitochondrial dysfunction of RPE in AMD (Iacovelli et al., 2016; Satish et al., 2018; Rosales et al., 2019; Shu et al., 2020, 2021). Despite evidence for both inflammation and metabolic dysfunction in AMD, there is a paucity of literature dissecting the crosstalk between these two mechanisms in the AMD field. Hence, this study sought to examine whether TNF α -driven inflammation in RPE is accompanied by changes in mitochondria and metabolism. Further, we investigated the efficacy of the fumaric acid ester, dimethyl fumarate (DMFu), in blocking TNF α -driven inflammation and metabolic changes in RPE.

Fumaric acid esters have been used as anti-inflammatory treatments for the autoimmune disease, psoriasis, for over 20 years (Blair, 2018). DMFu is FDA-approved for the treatment of relapsing multiple sclerosis in the form of delay-release capsules for oral use (Cada et al., 2013). DMFu is rapidly hydrolyzed to its active metabolite, monomethyl fumarate (MMF), which has a terminal half-life of 1 h. MMF is then metabolized by the TCA cycle to fumaric acid, citric acid, glucose, and carbon dioxide. The potent anti-inflammatory effect of DMFu is linked to its ability to block the NF- κ B pathway (Borgers et al., 2001), a downstream target of TNF α activation.

Here, we bridge the gap between inflammation and metabolic dysfunction in RPE showing that the pro-inflammatory effects of TNF α are associated with a dramatic change in mitochondrial morphology, function, and rewiring of the metabolic pathways. We reveal that pre-treatment of primary human RPE with the metabolic drug, DMFu, blocks the pro-inflammatory effects of TNF α , further highlighting the intertwined link between inflammation and metabolism.

MATERIALS AND METHODS

Cell Culture

Primary human fetal retinal pigment epithelial cells (H-RPE, Lonza Cat #00194987) were cultured in RtEGM Retinal Pigment Epithelial Cell Growth Medium supplemented with RtEGM SingleQuots (Lonza, Walkersville, MD, United States) as described previously (Shu et al., 2021). H-RPE were maintained at 37°C and 5% CO₂ in a humidified incubator and passaged 1:3 at a maximum of 5 passages. Half media changes for H-RPE were performed every 2–4 days for a month to ensure proper RPE maturation and pigment accumulation. Cells were serum starved for 2–3 days before treatment for up to 5 days with recombinant human TNF α (Peprotech, Rocky Hill, NJ, United States) at 10 ng/mL and/or 80 μ M dimethyl fumarate (242926, Sigma, St Louis, MO, United States) dissolved in the vehicle control, DMSO at the equivalent concentration of 0.04% (D4540, Sigma, St Louis, MO, United States). Brightfield images were captured on the EVOS M7000 Imaging System (Invitrogen, ThermoFisher, Waltham, MA, United States). Cells were tested monthly for mycoplasma contamination using the Mycoplasma PCR test (Applied Biological Materials, Cat #G238).

Quantitative PCR

Quantitative PCR (qPCR) assays were performed as previously described (Shu et al., 2021). Briefly, the E.Z.N.A. total RNA Kit I (Omega BioTek, Norcross, GA, United States) was used to extract total RNA and concentrations were determined using the NanoDrop Spectrophotometer ND-1000 (ThermoFisher Scientific, San Jose, CA, United States). cDNA synthesis was performed using the SuperScript IV VIL0 MasterMix and the Techne TC-512 Thermal Cycler at 25°C, 10 min; 50°C, 10 min; 85°C, 5 min (ThermoFisher Scientific, San Jose, CA, United States) and amplified by real-time PCR using the PowerUp SYBR Green Master Mix (ThermoFisher Scientific, San Jose, CA, United States) in a LightCycler 480 (Roche, Basel, Switzerland). Reactions were run in duplicate under the following thermal cycling conditions: 50°C, 2 min; 95°C, 2 min, followed by 40 cycles of 95°C for 15 s and 60°C for 1 min. Melt curve analysis was performed to confirm amplification specificity. *Ct* values were normalized to the housekeeping gene, TATA-binding protein (TBP), using the second derivative maximum method. Primer sequences are listed in **Table 1**.

High-Resolution Respirometry

The Seahorse XFe96 Analyzer (Agilent Technologies, Santa Clara, CA, United States) was used to determine real-time bioenergetic profiles. 20,000 H-RPE cells were seeded per well according to the manufacturer's instructions. For the Mito Stress Test, the medium was replaced with the assay medium (Seahorse XF Base Medium without Phenol Red, Agilent) supplemented with 2 mM GlutaMAX (ThermoFisher), 1 mM pyruvate (Gibco, Carlsbad, CA, United States) and 25 mM glucose (Sigma, St.

TABLE 1 | Primer sequences for qPCR.

Gene symbol	Gene name	Forward sequence (5'-3')	Reverse sequence (5'-3')
<i>ATP5O</i>	ATP synthase subunit O	TTTGAATCCCTATGTGAAGCGTT	CCTTGGGTATTGCTTAATCGACC
<i>C3</i>	Complement component 3	ACGGCCTTTGTCTCATCTC	CAAGGAAGTCTCCTGCTTTAGT
<i>CFB</i>	Complement factor B	GCTGTGAGAGAGATGCTCAATA	GACTCACTCCAGTACAAG
<i>CFH</i>	Complement factor H	CTGATCGCAAGAAAGACCAGTA	TGGTAGCACTGAACGGAATTAG
<i>IL-6</i>	Interleukin-6	ACTCACCTCTTCAGAACGAATTG	CCATCTTTGGAAGGTTCAAGTTG
<i>IL-8</i>	Interleukin-8	TTTTGCCAAGGAGTGCTAAAGA	AACCCTCTGCACCCAGTTTTTC
<i>MCP-1</i>	Monocyte chemoattractant protein-1	CAGCCAGATGCAATCAATGCC	TGGAATCCTGAACCCACTTCT
<i>PFKFB3</i>	6-phosphofructo-2-kinase/fructose-2,6-biphosphatase 3	CAGTTGTGCCTCCAATATC	GGCTTCATAGCAACTGATCC
<i>PGC-1A</i>	Peroxisome proliferator-activated receptor gamma, coactivator 1 alpha (PPARGC1A)	GTCACCACCCAAATCCTTAT	ATCTACTGCCTGGAGACCTT
<i>PKM2</i>	Pyruvate kinase muscle isozyme M2	CAAAGGACCTCAGCAGCCATGTC	GGGAAGCTGGGCCAATGGTACAGA
<i>VEGFA</i>	Vascular endothelial growth factor A	GGGCAGAATCATCACGAAGTG	ATTGGATGGCAGTAGCTGCG
<i>VEGFC</i>	Vascular endothelial growth factor C	GCCAATCACACTTCCTGCCGAT	AGGTCTTGTTCGCTGCCTGACA
<i>TBP</i>	TATA-binding protein	TGCACAGGAGCCAAGAGTGAA	CACATCACAGCTCCCCACCA

Louis, MO, United States), pH 7.4 and placed in a 37°C, CO₂-free, humidified incubator for 1 h. The drug injections were oligomycin (2.5 μM), BAM15 (10 μM) and a combination of rotenone and antimycin A (both at 2 μM). The same reagents were used for the ATP Rate Assay with the BAM15 drug injection excluded. For the Glycolytic Stress Test, the medium was replaced with the assay medium (Seahorse XF Base Medium without Phenol Red, Agilent) supplemented with 1 mM GlutaMAX (ThermoFisher), pH 7.4, and placed in a 37°C, CO₂-free, humidified incubator for 1 h. The drug injections were glucose (10 mM), oligomycin (2 μM), and 2DG (50 mM). On completion of the Seahorse assays, cells were lysed in cold 1× Cell Lysis Buffer (Cell Signaling Technology, Beverly, MA, United States) supplemented with 1 mM PMSF (Sigma, St Louis, MO, United States) and stored at -80°C. Protein concentration was quantified using the Pierce BCA Assay kit (ThermoFisher, Waltham, MA, United States). Data were normalized to protein content using the XF Wave software by exporting the XF Mito Stress Test, XF Glycolytic Stress Test and XF ATP Rate Assay Test Report Generators to Excel and GraphPad Prism.

Oxygen Consumption Rate (OCR) was also measured using the Resipher (Lucid Scientific, Atlanta, GA, United States). 50,000 H-RPE cells were seeded into the Falcon flat-bottom 96-well microplate (Corning #353072) in H-RPE culture medium with the Resipher oxygen sensing lid. Cells were serum starved for 2 days before treatment with TNFα at 10 ng/ml. Real-time continuous OCR measurements were monitored in the incubator for a week. Data were analyzed using the Resipher web application and Python.

Measurement of Intracellular ATP Content

ATP content was measured using the ATP bioluminescence assay kit CLS II (Roche, Heidelberg, Germany) as previously described (Shu et al., 2021). Protein content was measured using the Pierce BCA Assay kit. 20 μg of protein was run in duplicate in a white, flat-bottom 96-well microplate. Determination of free ATP

was performed against an ATP standard curve. Luminescence was determined at 60 ms integration using a Synergy H1 Plate Reader (BioTek, Winooski, VT, United States).

Quantification of Mitochondrial Copy Number

Genomic DNA (gDNA) was isolated using the Universal Genomic DNA Kit (CWBio #CW2298S). DNA concentration and purity was measured using the NanoDrop Spectrophotometer ND-1000. 10 ng of gDNA was used for the qPCR reactions and performed as previously described (Shu et al., 2021) using the Clontech Human Mitochondrial DNA (mtDNA) Monitoring Primer Set (Takara Bio Inc., Kusatsu, Shiga, Japan). mtDNA copy number was calculated as the average of the ratio of mtDNA to nuclear DNA using the two pairs of genes mt-*ND5* with *SERPINA1* and *ND1* with *SLCO2B1*.

Transmission Electron Microscopy

Cells were fixed with quarter strength Karnovsky's fixative (1% formaldehyde + 1.25% glutaraldehyde, in 0.1 M sodium cacodylate buffer, pH 7.4) for 6 h at room temperature, then transferred into 0.1 M sodium cacodylate buffer, post-fixed with 1% osmium tetroxide in 0.1 M sodium cacodylate buffer for 1 h, en bloc stained with 1% gadolinium triacetate in 0.05 M sodium maleate buffer, 4-6°C, pH 6 for 30 min. Samples were dehydrated with graded ethyl alcohol solutions, transitioned with propylene oxide and infiltrated in tEPON-812 epoxy resin (Tousimis, Rockville, MD, United States) utilizing an automated EMS Lynx 2 EM tissue processor (Electron Microscopy Sciences, Hatfield, PA, United States). The processed samples were oriented into tEPON-812 epoxy resin inside flat molds and polymerized using an oven set at 60°C. The polymerized blocks were cleaved from the coverglass through brief exposure in liquid nitrogen. Semi-thin sections were cut at 1 μm thickness and stained with 1% toluidine blue in 1% sodium tetraborate aqueous solution for assessment by light microscopy. A region containing a monolayer of cells was selected from each sample from the semi-thin toluidine blue stained sections and block face trimmed

to $<1 \text{ mm} \times 0.5 \text{ mm}$ for ultramicrotomy. Ultrathin sections (80 nm) were cut from each block face using a Leica EM UC7 ultramicrotome (Leica Microsystems, Buffalo Grove, IL, United States) and diamond knives (Diatome, Hatfield, PA, United States), to collect onto $2 \times 1 \text{ mm}$, single slot formvar-carbon coated grids and 200 mesh copper/rhodium uncoated grids (Electron Microscopy Sciences, Hatfield, PA, United States). The ultrathin sections on grids were stained with aqueous 2.5% gadolinium triacetate and modified Sato's lead citrate using a modified Hiraoka grid staining system (Seifert, 2017). Grids were imaged using a FEI Tecnai G2 Spirit transmission electron microscope (FEI, Hillsboro, OR, United States) at 80 kV interfaced with an AMT XR41 digital CCD camera (Advanced Microscopy Techniques, Woburn, MA, United States) for digital TIFF file image acquisition. All TEM digital images were captured at $2\text{k} \times 2\text{k}$ pixels at 16-bit resolution with the same magnification. Images were processed using Contrast Limited AHE (CLAHE) on ImageJ to reduce background noise and amplify mitochondrial ultrastructural features. Images were further analyzed on ImageJ using the hand-trace tool to obtain the area of the mitochondria.

Statistical Analysis

Statistical analyses were performed using GraphPad Prism 9.1.1. Parametric data were analyzed by one-way ANOVA with Tukey's *post hoc* analysis or unpaired Student's *t*-test. Statistical significance was considered when $p \leq 0.05$ and all data are shown as mean \pm SEM. * $p \leq 0.05$, ** $p \leq 0.01$, *** $p \leq 0.001$, and **** $p \leq 0.0001$.

RESULTS

Tumor Necrosis Factor-Alpha-Induced Inflammation in Retinal Pigment Epithelial Cells Is Accompanied by Mitochondrial Dysfunction

TNF α induced H-RPE elongation after 5 days of treatment (Figure 1A) while triggering a rapid inflammatory response with increased IL-6 secretion (Figure 1B) and increased gene expression of pro-inflammatory cytokines (IL-6, IL-8, and MCP-1) at 24 h (Figure 1C). This pro-inflammatory activation of RPE by TNF α was accompanied by the repression of PGC-1 α , a master regulator of RPE mitochondrial function and homeostasis, at 24 h (Figure 1D). Ultrastructural analysis showed that TNF α induced a dramatic enlargement of mitochondria and cristae sparsity at 5 days as observed by TEM imaging (Figure 1E). Quantification of mitochondrial area showed that TNF α -treated cells displayed a higher frequency of larger mitochondria (Figure 1F) and a significantly larger average mitochondrial area (Figure 1G).

Tumor Necrosis Factor-Alpha Increased Mitochondrial Respiration and Reduced Glycolysis in Retinal Pigment Epithelial Cells

Given the aberrant mitochondrial morphology observed, we next investigated whether TNF α induced any changes in

mitochondrial function by assessing RPE bioenergetics on the Seahorse XFe96 Mito Stress Test. Enlarged mitochondrial size typically confers enhanced bioenergetic capacity (Westermann, 2012). Accordingly, the larger mitochondria observed with TNF α was associated with a significantly increased basal respiration, maximal respiration, ATP production, and spare respiratory capacity (SRC) at 5 days (Figures 2A,B). TNF α also significantly increased coupling efficiency (Figure 2C). In contrast, TNF α reduced glycolysis and glycolytic capacity with a slight elevation of glycolytic reserve (Figures 2D,E). Consistent with the fact that OXPHOS is far more efficient at generating ATP compared to glycolysis, the increased mitochondrial respiration with TNF α was accompanied by a significant increase in intracellular ATP content at 5 days (Figure 2F). Furthermore, the Seahorse ATP rate assay confirmed the enhanced OXPHOS with TNF α , highlighting that a higher proportion of ATP generation was derived from mitochondrial respiration than glycolysis (Figures 2G,H), further indicated by the significantly higher ATP rate index (Figures 2I,J). Continuous monitoring of oxygen flux of H-RPE in the incubator using the Resipher confirmed the elevated OCR with TNF α (Figure 2K) with increasingly significant OCR elevations over time from 24 to 96 h (Figure 2L).

Pre-treatment With Dimethyl Fumarate Blocks Tumor Necrosis Factor-Alpha-Induced Inflammation and Restores Mitochondrial Health

Pre-treatment with DMFu for 2 h prior to TNF α exposure blocked TNF α -induced cellular elongation, maintaining the regular cobblestone-like epithelial morphology (Figure 3A). DMFu alone did not affect cellular morphology (Figure 3A). DMFu significantly suppressed TNF α -induced IL-6 secretion at both 24 h (Figure 3B) and 5 days (Figure 3C). Moreover, DMFu reduced gene expression of inflammatory cytokines including IL-6 (Figure 3D), IL-8 (Figure 3E), and MCP-1 (Figure 3F) at 24 h and 5 days.

Local activation and induction of the alternative complement cascade, an integral part of innate immunity, has been implicated in AMD pathogenesis (Johnson et al., 2001). At 24 h, TNF α robustly enhanced the gene expression of key components of the alternative complement cascade including complement factor H (CFH, Figure 4A), complement factor B (CFB, Figure 4B), and complement component 3 (C3, Figure 4C), which were all significantly suppressed with DMFu pre-treatment. There were no significant changes observed for complement factor I (CFI, Figure 4D).

A critical driver of late-stage neovascular AMD is the pro-angiogenic factor, vascular endothelial growth factor (VEGF) (Rosenfeld et al., 2006). Polarized VEGF expression is important for RPE homeostasis and survival (Ford et al., 2011). Specifically, VEGF-A expression by RPE is essential for choriocapillaris maintenance, and RPE dedifferentiation is associated with loss of VEGF secretion and choriocapillaris dropout (Blaauwgeers et al., 1999; Saint-Geniez et al., 2009). TNF α significantly reduced VEGF-A gene expression at 5 days while pre-treatment with DMFu maintained basal VEGF-A levels (Figure 4E). No

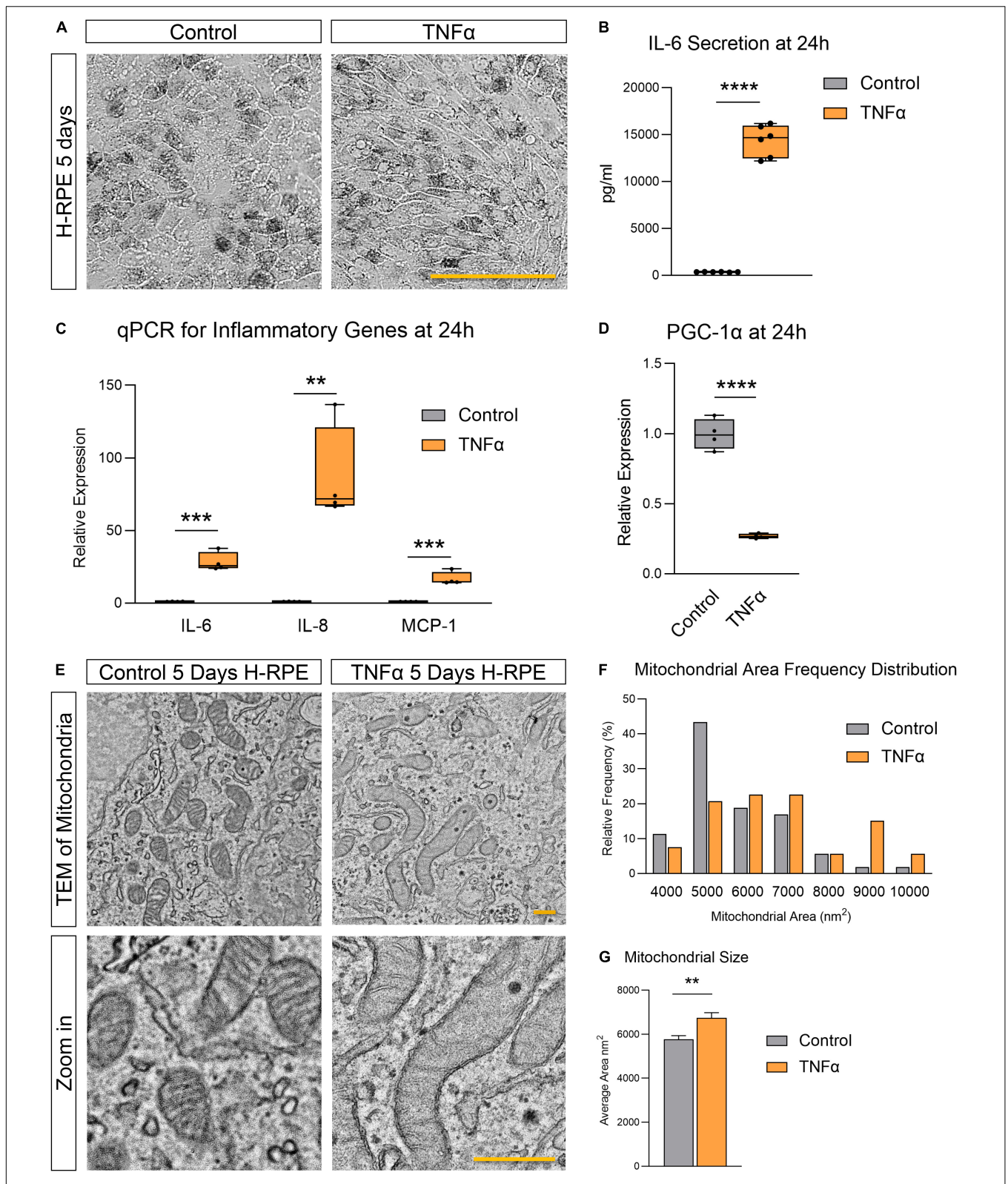


FIGURE 1 | Tumor necrosis factor-alpha-induced inflammation in H-RPE is accompanied by mitochondrial dysfunction. **(A)** Brightfield images of H-RPE cells with and without TNF α treatment. **(B)** IL-6 secretion at 24 h measured using ELISA for H-RPE. **(C,D)** qPCR analysis of inflammatory **(C)** and PGC-1 α **(D)** gene expression in H-RPE following 24 h treatment with TNF α . **(E)** TEM images of H-RPE comparing untreated control and TNF α -treatment for 5 days. **(F)** Quantification of mitochondrial size from TEM images presented as a frequency distribution histogram, and **(G)** quantification of average mitochondrial size (unpaired *t*-test). Error bars are means \pm SEM. ** $p \leq 0.01$; *** $p \leq 0.001$; **** $p \leq 0.0001$; ns, not significant. Scale bar for panel **(A)** is 100 μ m and panel **(E)** is 500 nm.

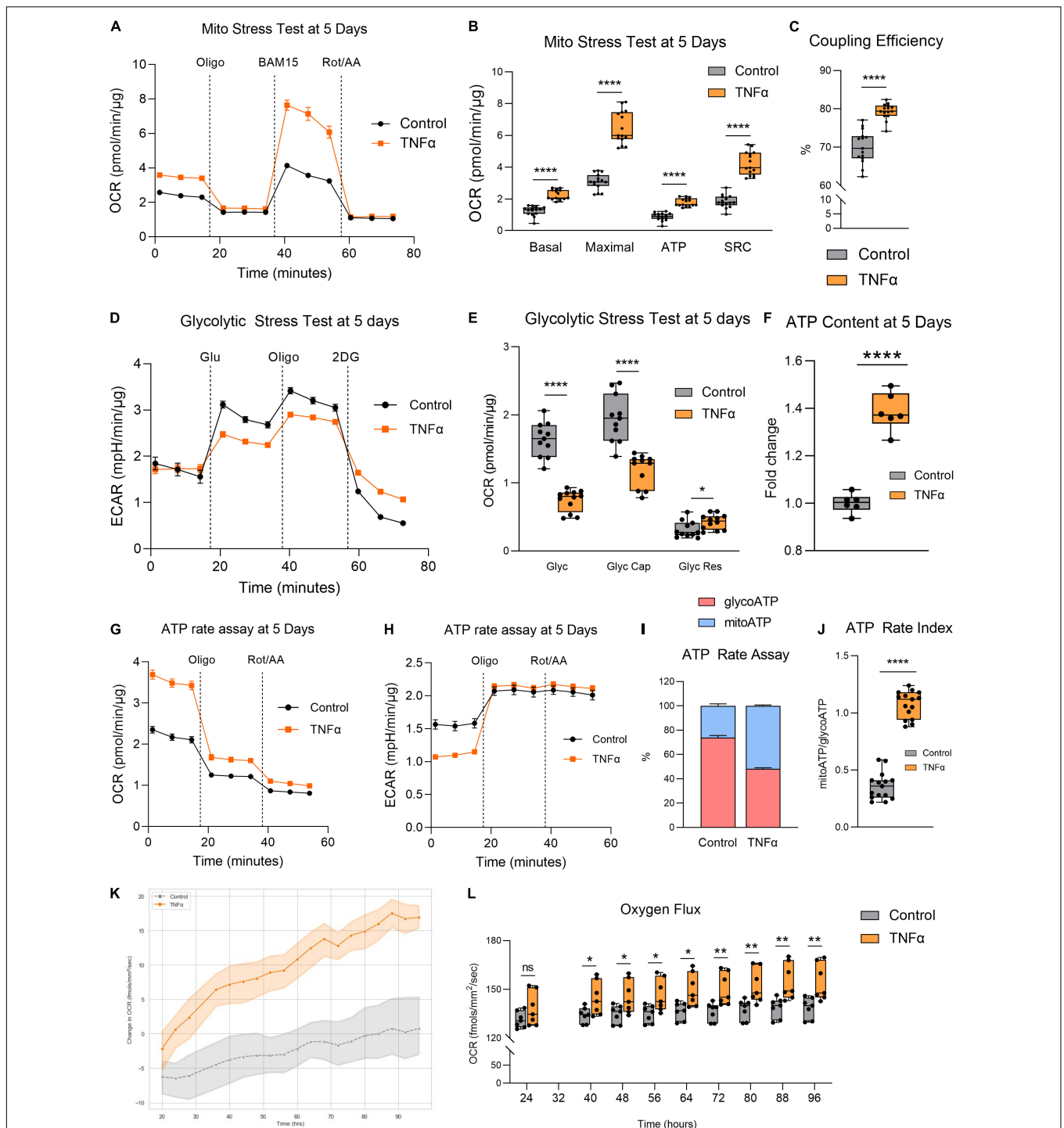
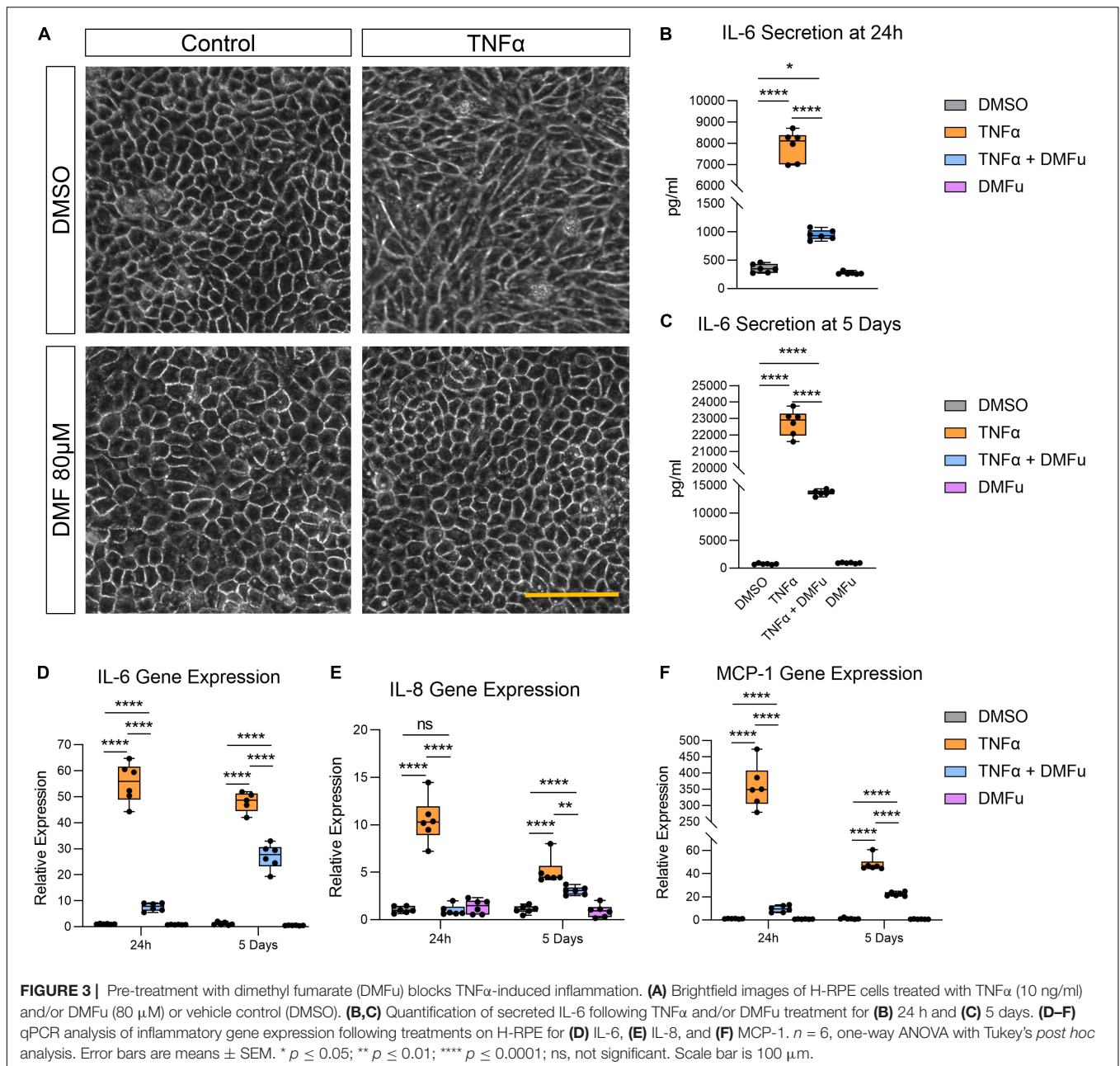


FIGURE 2 | Tumor necrosis factor- α increased mitochondrial respiration and reduced glycolysis in RPE. **(A)** Real-time measurement of oxygen consumption rate (OCR) using the Seahorse XFe96 BioAnalyzer to assess **(B)** OXPHOS parameters: basal respiration, ATP-linked respiration, proton leak, spare respiratory capacity (SRC), and maximal respiration based on responses to drug injections of oligomycin (Oligo), BAM15, and rotenone and antimycin A (Rot/AA) at 5 days with and without TNF α ($n = 10-12$, unpaired t -test) and **(C)** coupling efficiency. **(D)** Real-time measurement of extracellular acidification rate (ECAR) using the Seahorse XFe96 BioAnalyzer to assess glycolytic function parameters: **(E)** glycolysis, glycolytic capacity, and glycolytic reserve based on responses to drug injections of glucose (Glu), oligomycin (Oligo), and 2-deoxyglucose (2DG) at 5 days of treatment with and without TNF α ($n = 10-12$, unpaired t -test). **(F)** Intracellular ATP content at 5 days with or without TNF α ($n = 6$, unpaired t -test). **(G)** OCR curves and **(H)** ECAR curves for the Seahorse ATP rate assay at 5 days with TNF α . **(I)** Proportion of mitochondria-derived ATP production and glycolysis-derived ATP production and **(J)** increased ATP Rate Index representing a more oxidative and less glycolytic phenotype with TNF α treatment. **(K)** Real-time monitoring of OCR using the Respiher technology over 96 h following treatment with TNF α and **(L)** quantification of OCR over time ($n = 7$, unpaired t -test). Error bars are means \pm SEM. * $p \leq 0.05$; ** $p \leq 0.01$; **** $p \leq 0.0001$; ns, not significant.



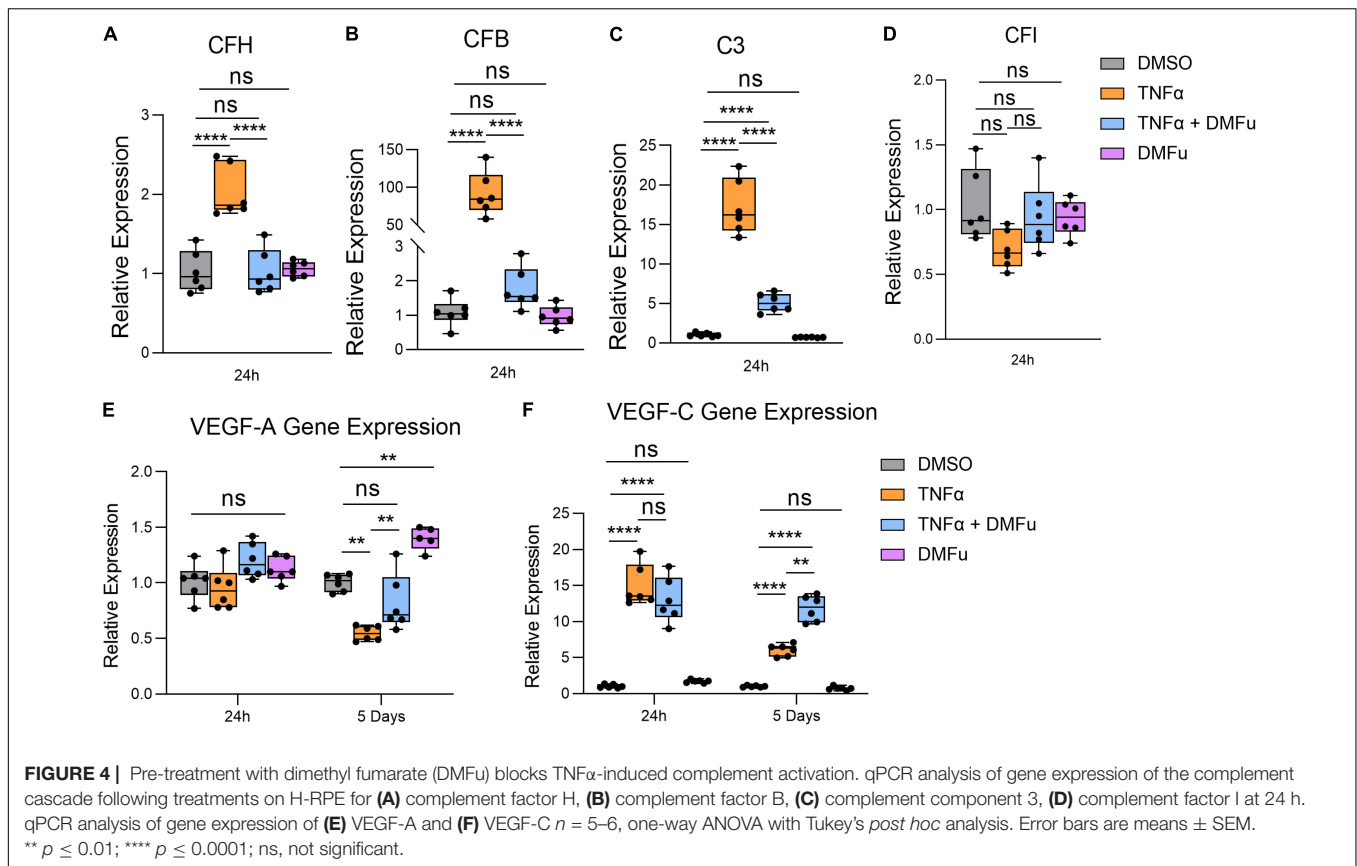
significant changes for VEGF-A occurred at 24 h (**Figure 4E**). VEGF-C is a potent enhancer of vascular permeability and has been identified in RPE derived from choroidal neovascular (CNV) specimens from patients (Martin et al., 2004). VEGF-C gene expression was increased with TNF α at both 24 h and 5 days and appeared to be further increased in the presence of DMFu (**Figure 4F**).

The anti-inflammatory activity of DMFu was accompanied by a shift toward normalized mitochondrial function. While TNF α increased mtDNA copy number, co-treatment with TNF α and DMFu reduced mtDNA copy number down to basal levels (**Figure 5A**). Similarly, co-treatment with TNF α and DMFu significantly enhanced PGC-1 α levels compared to TNF α alone;

however, this was not sufficient to maintain basal levels of PGC-1 α (**Figure 5B**). On an ultrastructural level, DMFu blocked TNF α -induced loss of cristae architecture and maintained normal mitochondrial size (**Figure 5C**).

Pre-treatment With Dimethyl Fumarate Blocks Tumor Necrosis Factor-Alpha-Induced Metabolic Reprogramming

On the Seahorse Mito Stress Test, DMFu blocked the elevated mitochondrial respiration induced by TNF α (**Figure 6A**). Specifically, DMFu blocked TNF α -dependent elevation of basal



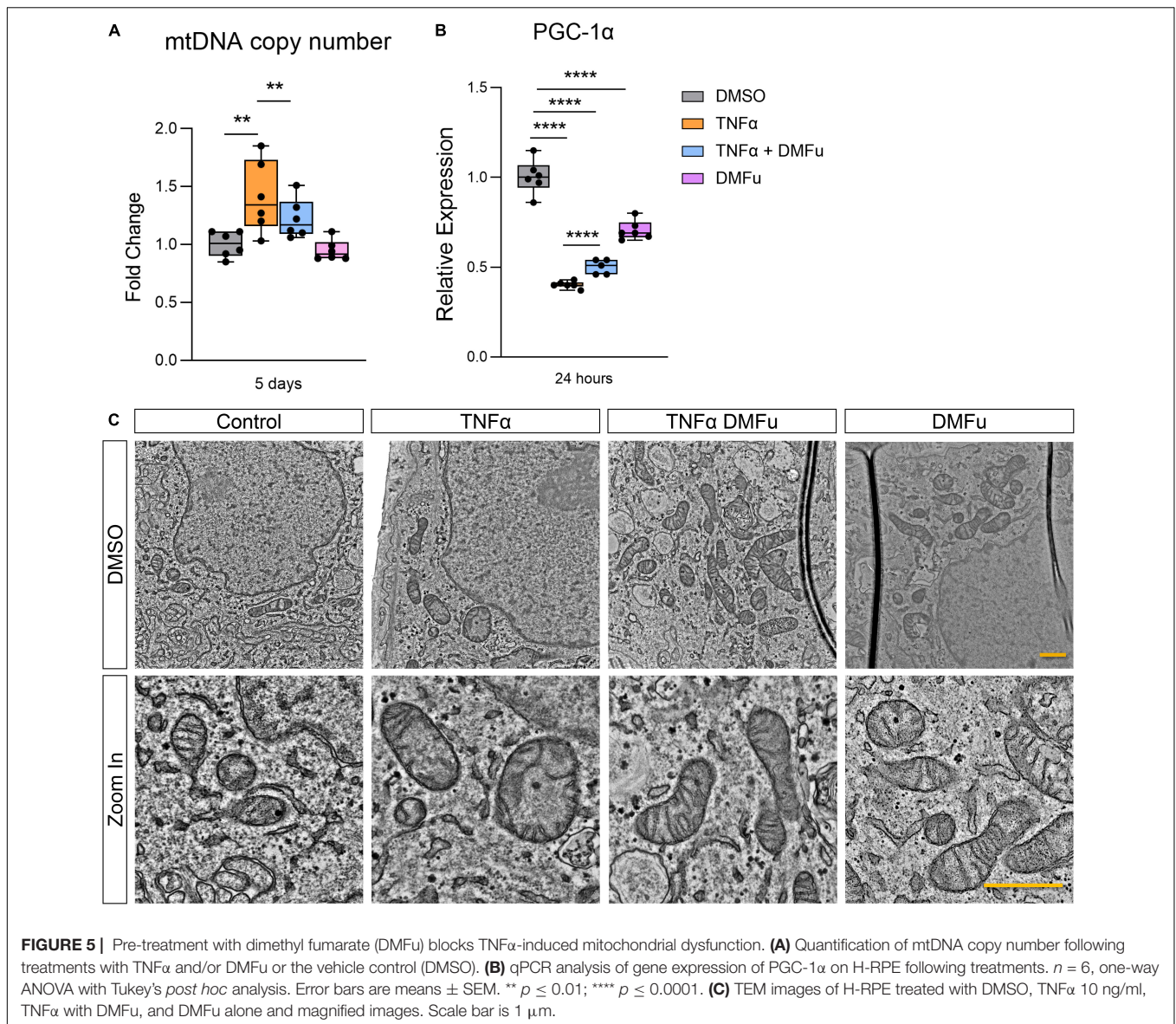
respiration (Figure 6B), maximal respiration (Figure 6C), ATP production (Figure 6D), spare respiratory capacity (Figure 6E), and coupling efficiency (Figure 6F). This blockade was accompanied by a reduction in gene expression of ATP5O, a key component of ATP synthase in the electron transport chain (Figure 6G). The Seahorse Glycolytic Stress Test showed that DMFu restored the suppression of glycolysis induced by TNF α (Figure 6H) with a statistically significant increase in glycolysis (Figure 6I), but no changes in glycolytic capacity (Figure 6J) and a reduction in glycolytic reserve (Figure 6K). The enhanced glycolysis with co-treatment of DMFu and TNF α is supported by the enhanced gene expression of glycolytic enzymes, namely, PFKFB3 (Figure 6L) and PKM2 (Figure 6M).

DISCUSSION

TNF α -induced inflammation in H-RPE is accompanied by a dramatic disruption in normal mitochondrial morphology and metabolic function. We show that TNF α induces the accumulation of engaged mitochondria with loss of cristae integrity and overactive metabolic function, promoting increased mitochondrial respiration, ATP production and reduced glycolysis in H-RPE. Pre-treatment of H-RPE with DMFu blocked TNF α -induced inflammation and normalized metabolic function and mitochondrial ultrastructural morphology.

An intricate interplay exists between inflammation and metabolic dysfunction at sites of ongoing inflammation (Kominsky et al., 2010). The enhanced OXPHOS and increased ATP production induced by TNF α in our study highlights the substantial bioenergetic challenge required to mount an inflammatory response in RPE. Intriguingly, our previous work showed that TGF β 2, an important cytokine in AMD pathogenesis, induces the opposite metabolic changes in RPE with reduced OXPHOS and enhanced glycolysis, leading to an overall reduction in ATP content (Shu et al., 2021). Since TGF β 2 itself does not induce inflammation, it is possible that the enhanced OXPHOS induced by TNF α may facilitate its pro-inflammatory activity. The capacity of RPE to switch between different bioenergetic profiles depending on cytokine stimulation shows the metabolic flexibility of RPE. Despite the capacity of both TGF β 2 and TNF α to induce robust EMT responses in RPE, a key component of pathogenic subretinal fibrosis in AMD (Shu et al., 2020, 2021), their divergent impact on metabolic reprogramming highlights the complexity of targeting metabolism as a therapeutic avenue for AMD. Future studies will continue to dissect the extensive crosstalk that exists between metabolism and EMT (Jia et al., 2021), examining how other metabolic pathways such as fatty acid oxidation and glutamine metabolism are impacted by TGF β 2 and TNF α in RPE.

Metabolic reprogramming of immune cells during activation is highly cell-type and context dependent. Divergent metabolic profiles have been observed with B and T lymphocytes with



B cells relying more on OXPHOS, while T cells rely more on aerobic glycolysis (Khalsa et al., 2019). Activation of B cells is bioenergetically demanding and consequently induces a progressive upregulation of OXPHOS to fulfill their new energy requirements (Price et al., 2018). Treatment of RPE with TNF α appears to mimic the metabolic changes observed in activated B cells. Indeed, activated B cells are known to secrete pro-inflammatory cytokines including TNF α and IL-6 (Gupta et al., 2013), which may, in turn, further potentiate inflammation and mitochondrial respiration. Our finding that TNF α increases OXPHOS in RPE has also been reported in platelets of aged mice where the pro-inflammatory activity of TNF α was linked to mitochondrial dysfunction, increased mitochondrial mass and metabolite rewiring to favor elevated pentose phosphate pathway intermediates (Davizon-Castillo et al., 2019). Future studies on comprehensive metabolomics analysis of TNF α -treated H-RPE

will determine the precise metabolic pathway reconfigurations, further unraveling the complex interplay between inflammation and the RPE metabolome.

Activation of the alternative pathway of the complement cascade has been implicated in the pathogenesis of AMD and in particular, geographic atrophy (Desai and Dugel, 2022). Our study shows that TNF α robustly upregulates critical components of the complement cascade and that DMFu is able to suppress TNF α -induced complement activation. Intriguingly, the ability of DMFu to suppress complement activation is accompanied by enhanced angiogenic gene expression. VEGF-C, an established pro-angiogenic factor and enhancer of vascular permeability, was strongly induced by TNF α and further upregulated in the presence of DMFu, indicating a potential risk for promoting an angiogenic response as observed in neovascular AMD. Complement inhibition is believed to induce a shift in

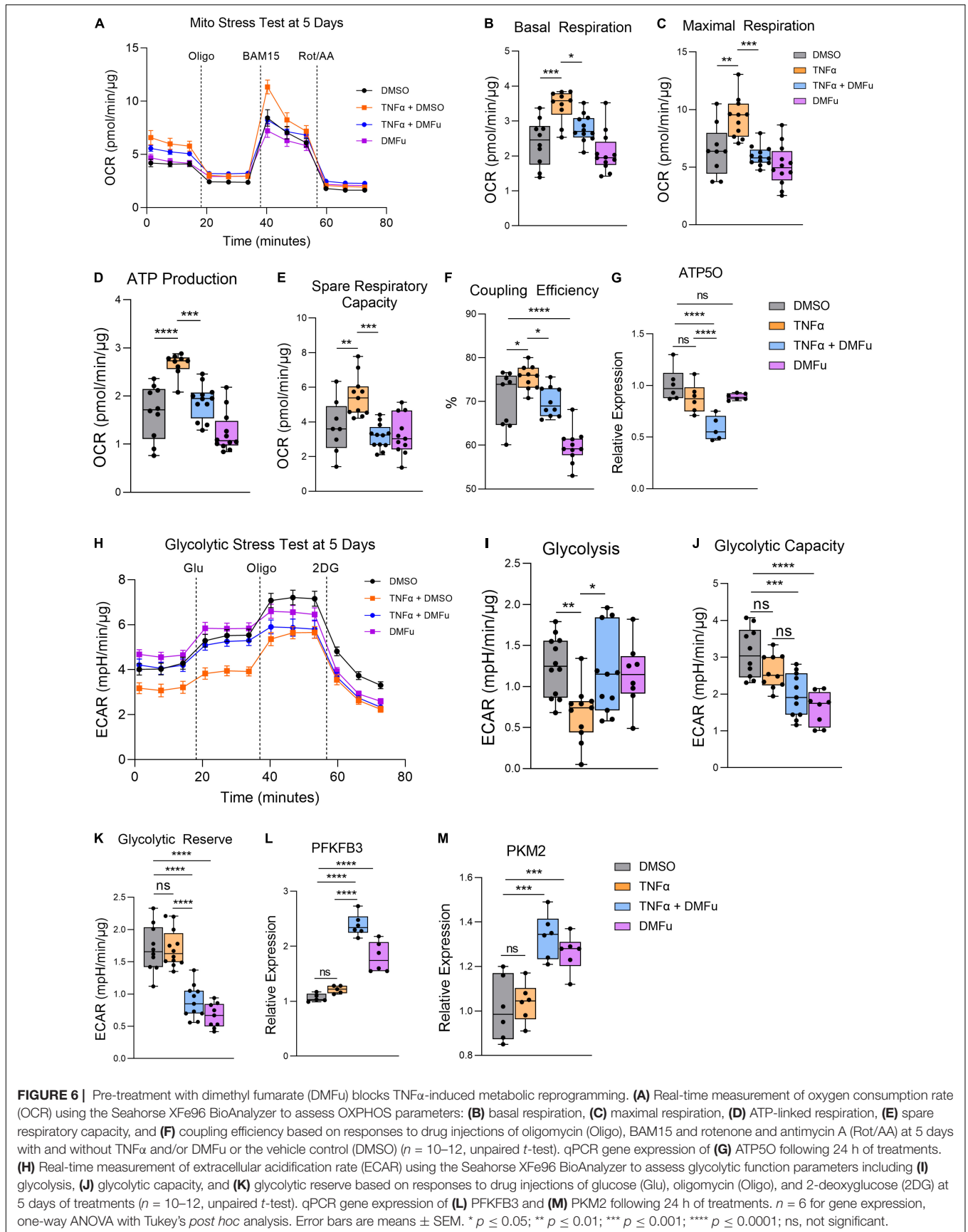


FIGURE 6 | Pre-treatment with dimethyl fumarate (DMFu) blocks TNF α -induced metabolic reprogramming. **(A)** Real-time measurement of oxygen consumption rate (OCR) using the Seahorse XFe96 BioAnalyzer to assess OXPHOS parameters: **(B)** basal respiration, **(C)** maximal respiration, **(D)** ATP-linked respiration, **(E)** spare respiratory capacity, and **(F)** coupling efficiency based on responses to drug injections of oligomycin (Oligo), BAM15 and rotenone and antimycin A (Rot/AA) at 5 days with and without TNF α and/or DMFu or the vehicle control (DMSO) ($n = 10-12$, unpaired t -test). qPCR gene expression of **(G)** ATP50 following 24 h of treatments. **(H)** Real-time measurement of extracellular acidification rate (ECAR) using the Seahorse XFe96 BioAnalyzer to assess glycolytic function parameters including **(I)** glycolysis, **(J)** glycolytic capacity, and **(K)** glycolytic reserve based on responses to drug injections of glucose (Glu), oligomycin (Oligo), and 2-deoxyglucose (2DG) at 5 days of treatments ($n = 10-12$, unpaired t -test). qPCR gene expression of **(L)** PFKFB3 and **(M)** PKM2 following 24 h of treatments. $n = 6$ for gene expression, one-way ANOVA with Tukey's *post hoc* analysis. Error bars are means \pm SEM. * $p \leq 0.05$; ** $p \leq 0.01$; *** $p \leq 0.001$; **** $p \leq 0.0001$; ns, not significant.

macrophage polarization from the pro-inflammatory M1 to the pro-angiogenic M2 macrophages (Cao et al., 2011). Indeed, in the clinical trial for the C3 inhibitor, APL-2, 18% of patients on monthly injections showed conversion to neovascular AMD, highlighting a critical link between complement inhibition and the risk of increased angiogenic potential (Park et al., 2019).

Our study highlights DMFu as a novel immunometabolic regulator of RPE. We show that the anti-inflammatory effect of DMFu was accompanied by a normalization of RPE metabolic function, blocking TNF α -induced elevated OCR and maintaining glycolysis at basal levels. The anti-inflammatory capacity of DMFu showed beneficial effects in an autoimmune uveitis rat model (Labsi et al., 2021) and optic neuritis murine model (Zyla et al., 2019). Further, DMFu promotes the survival of retinal ganglion cells (RGCs) after optic nerve crush (Mori et al., 2020) and protects against retinal degeneration in a light-induced photoreceptor loss mouse model (Dietrich et al., 2020). Mechanistically, studies have shown that DMFu activates Nrf2/heme oxygenase-1 (HO-1) (Zyla et al., 2019; Mori et al., 2020) and increases glutathione (Nelson et al., 1999; Dietrich et al., 2020) to mediate its anti-inflammatory and anti-oxidative effects. Intriguingly, in this study, DMFu alone induces significant metabolic changes compared to DMSO-treated control cells. For example, DMFu slightly reduces basal levels of PGC-1 α gene expression and increases the gene expression of glycolytic enzymes, PFKFB3 and PKM2, despite reducing glycolytic capacity and reserve. These metabolic changes do not impinge on the potent anti-inflammatory activity of DMFu against TNF α in RPE. The favorable efficacy and safety profiles of oral administration of DMFu for psoriasis and multiple sclerosis highlights its promise as a therapeutic avenue for immunomodulation of retinal diseases, including AMD. Furthermore, DMFu will only be considered as a treatment against active pathology rather than as a prophylactic therapy.

Ultrastructural mitochondrial imaging on TEM revealed dramatic mitochondrial defects following TNF α treatment of H-RPE, which was prevented by co-treatment with DMFu. Typically, long fused mitochondria are associated with enhanced OXPHOS capacity compared to smaller, fragmented mitochondria with reduced OXPHOS (Galloway et al., 2012). Indeed, our data shows that TNF α -induced elevated OXPHOS is associated with enlarged mitochondrial size, highlighting the morphological plasticity of RPE and reciprocal relationship between bioenergetic status and mitochondrial morphology. Elevated OXPHOS levels may generate more reactive oxygen species (ROS) byproducts that can cause further oxidative damage to mitochondrial morphology (Jassim et al., 2021). It is hypothesized that increased oxidative damage to mitochondria may lead to increased mtDNA copy number as an initial compensatory mechanism (Wang et al., 2014). Our data shows that TNF α increases mtDNA copy number in RPE, which can be blocked by co-treatment with DMFu. Similar results were observed in a clinical study of obese diabetic participants where increased body mass index (BMI) was associated with increased TNF α production, inflammation and mtDNA copy number (Skuratovskaia et al., 2019).

Our study reveals the dynamic interplay between inflammation and metabolic function in RPE, highlighting the morphological and bioenergetic alterations in mitochondria following TNF α stimulation. TNF α -driven inflammation causes a dramatic increase in energy demands in RPE, leading to increased oxygen consumption and ATP production at the expense of mitochondrial health. Such pro-inflammatory activation of RPE *in vivo* would undoubtedly cause an imbalance in the tightly regulated metabolic ecosystem of the retina (Kanow et al., 2017) through altered nutrient and oxygen availability for neighboring retinal cells. DMFu effectively abolished the drastic mitochondrial changes induced by TNF α , maintaining normal mitochondrial morphology and bioenergetic profiles and thus serves as a promising therapeutic avenue for combating inflammation in AMD.

DATA AVAILABILITY STATEMENT

The original contributions presented in this study are included in the article/supplementary material, further inquiries can be directed to the corresponding author.

AUTHOR CONTRIBUTIONS

DYS and MS-G: conceptualization and design. DYS, MS-G, SIF, and TCF: methodology. DYS, SIF, and MMK: writing—original draft preparation. DYS, SIF, TCF, ERB, and EN-J: formal analysis and investigation. DYS, SIF, TCF, MMK, ERB, EN-J, LAK, and MS-G: writing—review and editing. DYS, MS-G, and LAK: project administration and funding acquisition. All authors contributed to the article and approved the submitted version.

FUNDING

This study was supported in part by grants from the Fight for Sight Leonard & Robert Weintraub Postdoctoral Fellowship (DYS); BrightFocus Foundation Postdoctoral Fellowship Program in Macular Degeneration Research (M2021010F, DYS); Department of Defense, Spinal Vision Research Program under Award no. VR180132 (MS-G and LAK); National Eye Institute of the National Institutes of Health under Award no. R01EY027739 (LAK); the Grimshaw-Gudewicz Charitable Foundation (MS-G); The Iraty Award (MS-G); and the NEI Core Grant P30EYE003790.

ACKNOWLEDGMENTS

Acknowledgment is made to the donors of the Macular Degeneration Research M2021010F, a program of the BrightFocus Foundation, for support of this research. We thank Richard Bryan and Kin Lo for their assistance with the Resipher technology and data analysis. We also thank Philip Seifert at the Schepens Eye Research Institute (SERI) Morphology Core for electron microscopy assistance.

REFERENCES

- Ao, J., Wood, J. P., Chidlow, G., Gillies, M. C., and Casson, R. J. (2018). Retinal pigment epithelium in the pathogenesis of age-related macular degeneration and photobiomodulation as a potential therapy? *Clin. Exp. Ophthalmol.* 46, 670–686. doi: 10.1111/ceo.13121
- Blaauwgeers, H. G., Holtkamp, G. M., Rutten, H., Witmer, A. N., Koolwijk, P., Partanen, T. A., et al. (1999). Polarized vascular endothelial growth factor secretion by human retinal pigment epithelium and localization of vascular endothelial growth factor receptors on the inner choriocapillaris. evidence for a trophic paracrine relation. *Am. J. Pathol.* 155, 421–428. doi: 10.1016/S0002-9440(10)65138-3
- Blair, H. A. (2018). Dimethyl Fumarate: a review in moderate to severe plaque psoriasis. *Drugs* 78, 123–130. doi: 10.1007/s40265-017-0854-6
- Bonilha, V. L. (2008). Age and disease-related structural changes in the retinal pigment epithelium. *Clin. Ophthalmol.* 2, 413–424. doi: 10.2147/oph.s2151
- Borgers, M., Beyaert, R., Borghmans, I., Vandermeeren, M., Geysen, J., Wouters, H., et al. (2001). Dimethylfumarate is an inhibitor of cytokine-induced nuclear translocation of NF- κ B1, but not RelA in normal human dermal fibroblast cells. *J. Investig. Dermatol.* 116, 124–130. doi: 10.1046/j.1523-1747.2001.00211.x
- Cada, D. J., Levien, T. L., and Baker, D. E. (2013). Dimethyl fumarate. *Hosp. Pharm.* 48, 668–679.
- Cao, X., Shen, D., Patel, M. M., Tuo, J., Johnson, T. M., Olsen, T. W., et al. (2011). Macrophage polarization in the maculae of age-related macular degeneration: a pilot study. *Pathol. Int.* 61, 528–535. doi: 10.1111/j.1440-1827.2011.02695.x
- Chernykh, V., Shevchenko, A., Kononkov, V., Prokofiev, V., Eremina, A., and Trunov, A. (2019). TNF-alpha gene polymorphisms: association with age-related macular degeneration in Russian population. *Int. J. Ophthalmol.* 12, 25–29. doi: 10.18240/ijo.2019.01.04
- Datta, S., Cano, M., Ebrahimi, K., Wang, L., and Handa, J. T. (2017). The impact of oxidative stress and inflammation on RPE degeneration in non-neovascular AMD. *Prog. Retin. Eye Res.* 60, 201–218. doi: 10.1016/j.preteyeres.2017.03.002
- Davidon-Castillo, P., McMahon, B., Aguila, S., Bark, D., Ashworth, K., Allawzi, A., et al. (2019). TNF-alpha-driven inflammation and mitochondrial dysfunction define the platelet hyperreactivity of aging. *Blood* 134, 727–740. doi: 10.1182/blood.2019000200
- Desai, D., and Dugel, P. U. (2022). Complement cascade inhibition in geographic atrophy: a review. *Eye* 36, 294–302. doi: 10.1038/s41433-021-01765-x
- Dietrich, M., Hecker, C., Nasiri, M., Samsam, S., Issberner, A., Kohne, Z., et al. (2020). Neuroprotective properties of dimethyl fumarate measured by optical coherence tomography in non-inflammatory animal models. *Front. Neurol.* 11:601628. doi: 10.3389/fneur.2020.601628
- Fisher, C. R., and Ferrington, D. A. (2018). Perspective on AMD pathobiology: a bioenergetic crisis in the RPE. *Invest. Ophthalmol. Vis. Sci.* 59, AMD41–AMD47. doi: 10.1167/iov.18-24289
- Ford, K. M., Saint-Geniez, M., Walshe, T., Zahr, A., and D'Amore, P. A. (2011). Expression and role of VEGF in the adult retinal pigment epithelium. *Invest. Ophthalmol. Vis. Sci.* 52, 9478–9487. doi: 10.1167/iov.11-8353
- Galloway, C. A., Lee, H., and Yoon, Y. (2012). Mitochondrial morphology-emerging role in bioenergetics. *Free Radic. Biol. Med.* 53, 2218–2228. doi: 10.1016/j.freeradbiomed.2012.09.035
- Gupta, S., Agrawal, S., and Gollapudi, S. (2013). Increased activation and cytokine secretion in B cells stimulated with leptin in aged humans. *Immun. Ageing* 10:3. doi: 10.1186/1742-4933-10-3
- Hageman, G. S., Luthert, P. J., Victor Chong, N. H., Johnson, L. V., Anderson, D. H., and Mullins, R. F. (2001). An integrated hypothesis that considers drusen as biomarkers of immune-mediated processes at the RPE-Bruch's membrane interface in aging and age-related macular degeneration. *Prog. Retin Eye Res.* 20, 705–732. doi: 10.1016/s1350-9462(01)00010-6
- Iacovelli, J., Rowe, G. C., Khadka, A., Diaz-Aguilar, D., Spencer, C., Arany, Z., et al. (2016). PGC-1alpha induces human RPE oxidative metabolism and antioxidant capacity. *Invest. Ophthalmol. Vis. Sci.* 57, 1038–1051. doi: 10.1167/iov.15-17758
- Jassim, A. H., Inman, D. M., and Mitchell, C. H. (2021). Crosstalk between dysfunctional mitochondria and inflammation in glaucomatous neurodegeneration. *Front. Pharmacol.* 12:699623. doi: 10.3389/fphar.2021.699623
- Jia, D., Park, J. H., Kaur, H., Jung, K. H., Yang, S., Tripathi, S., et al. (2021). Towards decoding the coupled decision-making of metabolism and epithelial-to-mesenchymal transition in cancer. *Br. J. Cancer* 124, 1902–1911. doi: 10.1038/s41416-021-01385-y
- Johnson, L. V., Leitner, W. P., Staples, M. K., and Anderson, D. H. (2001). Complement activation and inflammatory processes in drusen formation and age related macular degeneration. *Exp. Eye Res.* 73, 887–896. doi: 10.1006/exer.2001.1094
- Kaarniranta, K., Uusitalo, H., Blasiak, J., Felszeghy, S., Kannan, R., Kauppinen, A., et al. (2020). Mechanisms of mitochondrial dysfunction and their impact on age-related macular degeneration. *Prog. Retin. Eye Res.* 79:100858. doi: 10.1016/j.preteyeres.2020.100858
- Kanow, M. A., Giarmarco, M. M., Jankowski, C. S., Tsantilas, K., Engel, A. L., Du, J., et al. (2017). Biochemical adaptations of the retina and retinal pigment epithelium support a metabolic ecosystem in the vertebrate eye. *Elife* 6:e28899. doi: 10.7554/eLife.28899
- Khalsa, J. K., Chawla, A. S., Prabhu, S. B., Vats, M., Dhar, A., Dev, G., et al. (2019). Functionally significant metabolic differences between B and T lymphocyte lineages. *Immunology* 158, 104–120. doi: 10.1111/imm.13098
- Khan, A. H., Pierce, C. O., De Salvo, G., Griffiths, H., Nelson, M., Cree, A. J., et al. (2021). The effect of systemic levels of TNF-alpha and complement pathway activity on outcomes of VEGF inhibition in neovascular AMD. *Eye* 8. doi: 10.1038/s41433-021-01824-3 [Epub ahead of print].
- Kominsky, D. J., Campbell, E. L., and Colgan, S. P. (2010). Metabolic shifts in immunity and inflammation. *J. Immunol.* 184, 4062–4068. doi: 10.4049/jimmunol.0903002
- Kutty, R. K., Samuel, W., Boyce, K., Cherukuri, A., Duncan, T., Jaworski, C., et al. (2016). Proinflammatory cytokines decrease the expression of genes critical for RPE function. *Mol. Vis.* 22, 1156–1168.
- Labsi, M., Soufli, I., Belguendouz, H., Djebbara, S., Hannachi, L., Amir, Z. C., et al. (2021). Beneficial effect of dimethyl fumarate on experimental autoimmune uveitis is dependent of pro-inflammatory markers immunomodulation. *Inflammopharmacology* 29, 1389–1398. doi: 10.1007/s10787-021-00864-1
- Levy, O., Calippe, B., Lavalette, S., Hu, S. J., Raoul, W., Dominguez, E., et al. (2015). Apolipoprotein E promotes subretinal mononuclear phagocyte survival and chronic inflammation in age-related macular degeneration. *EMBO Mol. Med.* 7, 211–226. doi: 10.15252/emmm.201404524
- Martin, G., Schlunck, G., Hansen, L. L., and Agostini, H. T. (2004). Differential expression of angioregulatory factors in normal and CNV-derived human retinal pigment epithelium. *Graefes Arch. Clin. Exp. Ophthalmol.* 42, 321–326. doi: 10.1007/s00417-003-0838-y
- Mori, S., Kurimoto, T., Maeda, H., and Nakamura, M. (2020). Dimethyl fumarate promotes the survival of retinal ganglion cells after optic nerve injury, possibly through the Nrf2/HO-1 pathway. *Int. J. Mol. Sci.* 22, 297. doi: 10.3390/ijms22010297
- Nelson, K. C., Carlson, J. L., Newman, M. L., Sternberg, P. Jr., Jones, D. P., Kavanagh, T. J., et al. (1999). Effect of dietary inducer dimethylfumarate on glutathione in cultured human retinal pigment epithelial cells. *Invest. Ophthalmol. Vis. Sci.* 40, 1927–1935.
- Oh, H., Takagi, H., Takagi, C., Suzuma, K., Otani, A., Ishida, K., et al. (1999). The potential angiogenic role of macrophages in the formation of choroidal neovascular membranes. *Invest. Ophthalmol. Vis. Sci.* 40, 1891–1898.
- Park, D. H., Connor, K. M., and Lambris, J. D. (2019). The challenges and promise of complement therapeutics for ocular diseases. *Front. Immunol.* 10:1007. doi: 10.3389/fimmu.2019.01007
- Price, M. J., Patterson, D. G., Scharer, C. D., and Boss, J. M. (2018). Progressive upregulation of oxidative metabolism facilitates plasmablast differentiation to a T-Independent antigen. *Cell. Rep.* 23, 3152–3159. doi: 10.1016/j.celrep.2018.05.053
- Rosales, M. A. B., Shu, D. Y., Iacovelli, J., and Saint-Geniez, M. (2019). Loss of PGC-1alpha in RPE induces mesenchymal transition and promotes retinal degeneration. *Life Sci. Alliance* 2:e201800212.
- Rosenfeld, P. J., Brown, D. M., Heier, J. S., Boyer, D. S., Kaiser, P. K., Chung, C. Y., et al. (2006). Ranibizumab for neovascular age-related macular degeneration. *N. Engl. J. Med.* 355, 1419–1431.
- Saint-Geniez, M., Kurihara, T., Sekiyama, E., Maldonado, A. E., and D'Amore, P. A. (2009). An essential role for RPE-derived soluble VEGF in the maintenance

- of the choriocapillaris. *Proc. Natl. Acad. Sci. U.S.A* 106, 18751–18756. doi: 10.1073/pnas.0905010106
- Satish, S., Philipose, H., Rosales, M. A. B., and Saint-Geniez, M. (2018). Pharmaceutical induction of PGC-1 α promotes retinal pigment epithelial cell metabolism and protects against oxidative damage. *Oxid. Med. Cell Longev* 2018:9248640. doi: 10.1155/2018/9248640
- Seifert, P. (2017). Modified hiraoka TEM grid staining apparatus and technique using 3D printed materials and gadolinium triacetate tetrahydrate, a non-radioactive uranyl acetate substitute. *J. Histotechnol.* 40, 130–135. doi: 10.1080/01478885.2017.1361117
- Shu, D. Y., Butcher, E., and Saint-Geniez, M. (2020). EMT and EndMT: emerging roles in age-related macular degeneration. *Int. J. Mol. Sci.* 21:4271. doi: 10.3390/ijms21124271
- Shu, D. Y., Butcher, E. R., and Saint-Geniez, M. (2021). Suppression of PGC-1 α drives metabolic dysfunction in TGF β 2-induced EMT of retinal pigment epithelial cells. *Int. J. Mol. Sci.* 22:4701. doi: 10.3390/ijms22094701
- Skuratovskaia, D., Zatolokin, P., Vulf, M., Mazunin, I., and Litvinova, L. (2019). Interrelation of chemerin and TNF- α with mtDNA copy number in adipose tissues and blood cells in obese patients with and without type 2 diabetes. *BMC Med. Genomics* 12:40. doi: 10.1186/s12920-019-0485-8
- Wan, L., Lin, H. J., Tsai, Y., Lee, C. C., Tsai, C. H., Tsai, F. J., et al. (2010). Tumor necrosis factor- α gene polymorphisms in age-related macular degeneration. *Retina* 30, 1595–1600. doi: 10.1097/IAE.0b013e3181dc58a6
- Wang, P. W., Kuo, H. M., Huang, H. T., Chang, A. Y., Weng, S. W., Tai, M. H., et al. (2014). Biphasic response of mitochondrial biogenesis to oxidative stress in visceral fat of diet-induced obesity mice. *Antioxid. Redox. Signal* 20, 2572–2588. doi: 10.1089/ars.2013.5334
- Westermann, B. (2012). Bioenergetic role of mitochondrial fusion and fission. *Biochim. Biophys. Acta* 1817, 1833–1838. doi: 10.1016/j.bbabi.2012.02.033
- Zhang, M., Jiang, N., Chu, Y., Postnikova, O., Varghese, R., Horvath, A., et al. (2020). Dysregulated metabolic pathways in age-related macular degeneration. *Sci. Rep.* 10:2464. doi: 10.1038/s41598-020-59244-4
- Zyla, K., Larabee, C. M., Georgescu, C., Berkley, C., Reyna, T., and Plafker, S. M. (2019). Dimethyl fumarate mitigates optic neuritis. *Mol. Vis.* 25, 446–461.
- Conflict of Interest:** The authors declare that the research was conducted in the absence of any commercial or financial relationships that could be construed as a potential conflict of interest.
- Publisher's Note:** All claims expressed in this article are solely those of the authors and do not necessarily represent those of their affiliated organizations, or those of the publisher, the editors and the reviewers. Any product that may be evaluated in this article, or claim that may be made by its manufacturer, is not guaranteed or endorsed by the publisher.
- Copyright © 2022 Shu, Frank, Fitch, Karg, Butcher, Nnuji-John, Kim and Saint-Geniez. This is an open-access article distributed under the terms of the Creative Commons Attribution License (CC BY). The use, distribution or reproduction in other forums is permitted, provided the original author(s) and the copyright owner(s) are credited and that the original publication in this journal is cited, in accordance with accepted academic practice. No use, distribution or reproduction is permitted which does not comply with these terms.